Contents lists available at ScienceDirect

Composites Part B

Tension, compression, and shear behavior of advanced sheet molding compound (A-SMC): Multi-scale damage analysis and strain rate effect

Mohammadali Shirinbayan [*], Hassan Beigi Rizi, Navideh Abbasnezhad, Abbas Tcharkhtchi, Joseph Fitoussi

Arts et Metiers Institute of Technology, CNRS, CNAM, PIMM, HESAM University, F-75013, Paris, France

A B S T R A C T

Advanced sheet molding compounds (A-SMC) are a new generation of alternative materials to steels for applying in automotive structures. It contains a thermoset matrix involving mineral charge ($CaCO_3$) reinforced with a high fraction of discontinuous bundles of glass fibers (around 50% in mass) compared to the other types of SMC composites. The crashworthiness evaluation and multi-scale mechanical characterizations of this automotive material is essential. In this study, at first, the microstructure of A-SMC composite was investigated by Scanning Electron Microscopy (SEM), ultrasonic analysis, and X-ray micro-tomography. Two configurations' plates of Randomly Oriented (RO) and Highly Oriented (HO) were analyzed under quasi-static tension, compression, and shear loadings. To study the effect of fiber orientation, for HO plate, two fiber directions were chosen: HO-0° (parallel to the Mold Flow Direction (MFD)) and HO-90° (perpendicular to the MFD). Strain rate effect (from 0.25 s^{-1} to 10 s^{-1}) on shear properties and visco-damage behavior of A-SMC composite has been studied. For this purpose, a new setup for shear testing was designed after optimization via ABAQUS FE code to achieve constant strain rate. HO-0° samples represented higher strength in tension and compression loadings, unlike shear loading compared to RO and HO-90° samples. A multi-scale damage study confirmed that predominant damage mechanism is decohesion at fiber/matrix interface under tension, compression, and shear loadings.

Authors' contributions

Mohammadali Shirinbayan: construct the idea, analyzed results, draft manuscript preparation, and wrote the paper, correct the English and the paper format. Hassan Beigi Rizi: analyzed results, draft manuscript preparation, and wrote the paper, correct the English and the paper format. Navideh Abbasnezhad: analyzed results, draft manuscript preparation, and wrote the paper, correct the English and the paper format. Abbas Tcharkhtchi: construct the idea: analyzed results, draft manuscript preparation, and wrote the paper. Joseph Fitoussi: construct the idea: analyzed results, draft manuscript preparation, and wrote the paper.

Availability of data and materials

The authors declare that the data and the materials of this study are available within the article.

1. Introduction

Zero- and Low-Emission Vehicles (ZLEV) have been the center of attention of automotive industries. Every few years, European Commission attends a session for setting a target of increasing lifetime service and reducing greenhouse gas emissions of a new generation of cars [1,2]. Consequently, one of the important factors is the type of applied materials. In this issue, Sheet Molding Compounds (SMCs) are an alternative to metallic parts thanks to lightweight, excellent chemical resistance, and long-life service for automotive structural components [3]. SMC composites are high-strength, cost-effective composites, with the combination of thermosetting resin (vinyl ester, phenolic, modified vinyl urethane and unsaturated polyester), fillers (calcium carbonate, clay, mica, etc.), fiber reinforcement (glass, carbon, or aramid fibers) and other additives for special aims that are manufactured by thermo-compression process [4,5]. Recently, a new generation of SMC composites called Advanced SMCs (A-SMCs) containing vinyl-ester resins

Table 1
A comparison between three types of SMC in terms of composition [2,36].

Composition	A-SMC (wt %)	LD-SMC (wt%)	Standard SMC (wt %)
Glass fibers	50%	30%	30%
Matrix	24% (Vinyl-ester resin)	(22% Hollow glass spheres+12% unsaturated polyester)	33% (Unsaturated polyester)
Filler	24% $CaCO_3$	32% $CaCO_3$	37% $CaCO_3$
Other additives	2%	4%	

with 50% chopped bundles of glass fibers in mass were introduced that possess impressive mechanical resistance and high energy absorption capacity compared to steels [6].

In an automobile, crashworthiness of structure is a capability for energy absorption of impact that should be considered in different aspects of damage via tension, compression, and shear loadings [7,8]. Designing the A-SMC composites similar to the other composites are challenging due to the variety of microstructure (i.e. amount of reinforcements and fibers orientation in addition to elastic, visco-elastic/plastic behavior of matrix), anisotropic behavior and multiple coupled damage mechanisms concerning to the condition of loading [9,10]. In this regard, a wide variety of studies were focused on their mechanical behavior in tension and compression loadings. Shirinbayan et al. [6] have developed an experimental procedure to study the mechanical behavior of A-SMC under high strain rate tensile test. The ABAQUS finite element (FE) code was used to simulate the optimal design of sample geometry and experimental damping set-up regarding
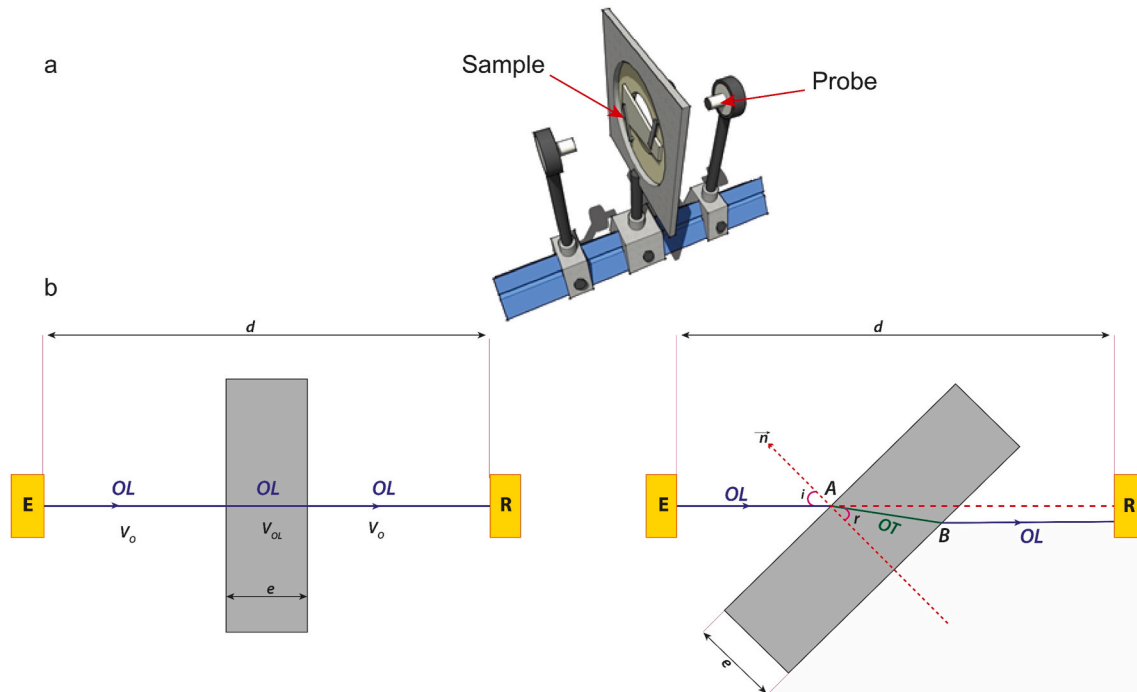

Fig. 1. A schematic of the ultrasonic method; (a) configuration of sample and probes, and (b) sample rotation for removing OL wave and appearing OT wave.
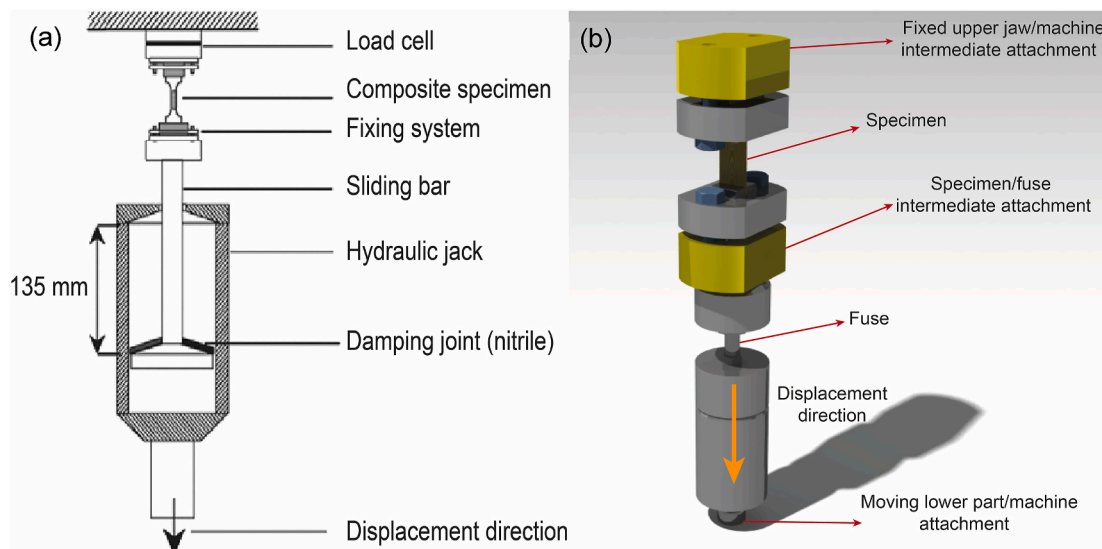

Fig. 2. Schematics of (a) high strain-rate tensile test, (b) interrupted tensile device [6].
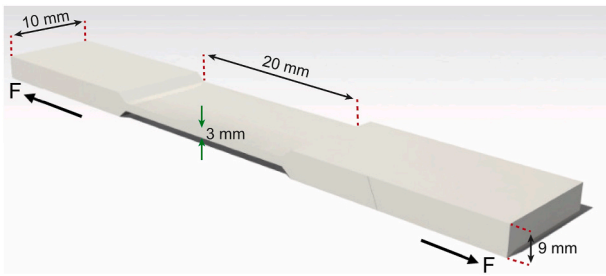
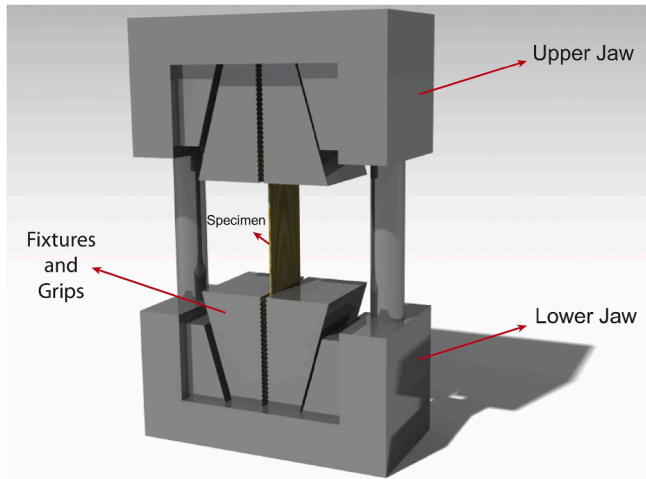**Fig. 3.** Dimensions of specimen for tensile test.

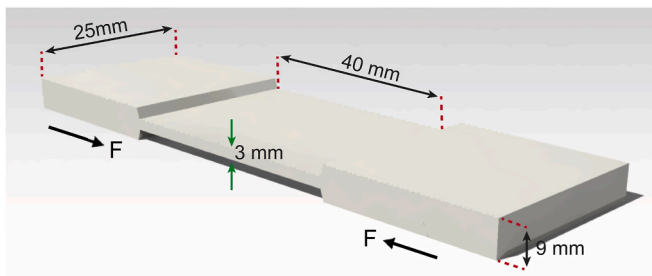**Fig. 4.** Schematic of testing set-up of compression jaw.

Fig. 5. Dimension of the specimen in the compression test.

the thickness and materials properties. A special attention was given to the multi-scale damage analysis of different fiber orientation of A-SMC under high strain rate loading. The results showed that the mechanical behavior of A-SMC composite was highly strain-rate dependent. However, Young's modulus presented a constant variation. Moreover, it was recognized that two damage mechanisms of fiber-matrix interface debonding and pseudo-delamination among the bundles of fibers were competing, which the latter was affected by strain rate and fiber orientation.

Likewise, in other study [3], the quasi-static and dynamic behavior of A-SMC composite for two configurations plates using interrupted tensile test method was studied. The outcomes revealed that the main mechanism of damage was fiber-matrix interface decohesion. At high strain rates, matrix micro-cracking that stems from interface micro-cracks propagation into the matrix in bundles of fibers was more obvious. One step before final failure, the mechanism of pseudo-delamination appeared, where it is more sensitive to high strain rates and fiber orientation parallel to the loading direction.

Besides of tensile test, modeling the compression behavior of SMC composites were more considered in the recent decade [11–15]. For example, Shirinbayan et al. [2], have studied the multi-scale damage analysis of low-density SMC (LD-SMC) composite for monitoring the consequences of local damage mechanisms in mechanical response of LD-SMCs under quasi-static compression loadings. The results confirmed the effect of fiber orientation on the compression behavior of LD-SMC. However, there is no study on the compression behavior of A-SMC composites.

In addition to tension and compression tests, shear behavior of composites is important [16,17]. Different shear test methods have been introduced like single lap shear testing (SLST) [18], short beam strength (SBS) shear testing [19,20] and compression shear test (CST) based on composite types. However, the mentioned tests contain some limitations. For better understanding, numerous studies were published in terms of shear test optimization [21–23]. Shokrieh et al. [24] carried out the investigation of in-plane shear properties dependency to strain rate from static to dynamic criterion via symmetric and balanced ±45° glass/epoxy composite laminate under uni-axial tensile test using a servo-hydraulic testing apparatus. They proved that shear properties were sensitive to strain rate. Holmes et al. [25] developed shear testing of woven thermoplastic composites through geometry optimization by designing an S-shaped specimen and provided a pure shear deformation mode for failure investigation. Moreover, Jia et al. [26] investigated the shear properties of polyurethane ductile adhesive in terms of strain rate dependency at a certain temperature. They applied thick adherent shear test (TAST) specimens and concluded that shear strength increased by loading speed. Kolanu et al. [27] studied damage assessment of carbon fiber reinforced polymers (CFRP) laminate, including cut-out part via
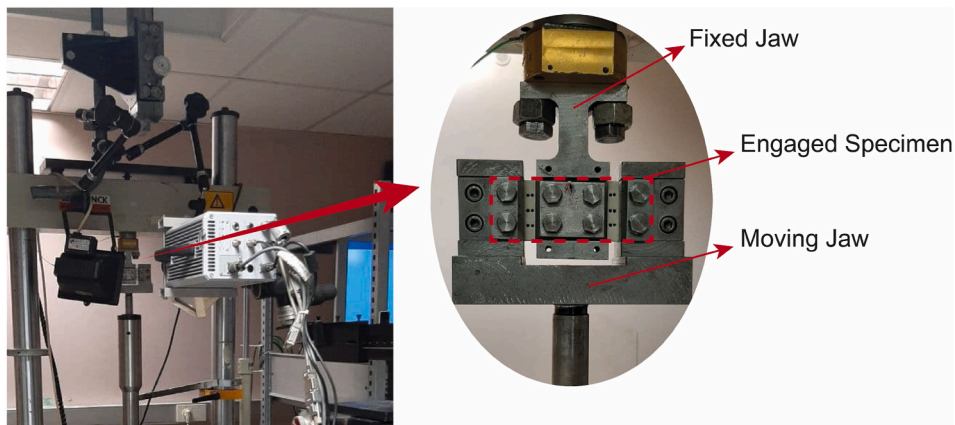

Fig. 6. Testing set-up for high strain shear behavior of A-SMC composite.
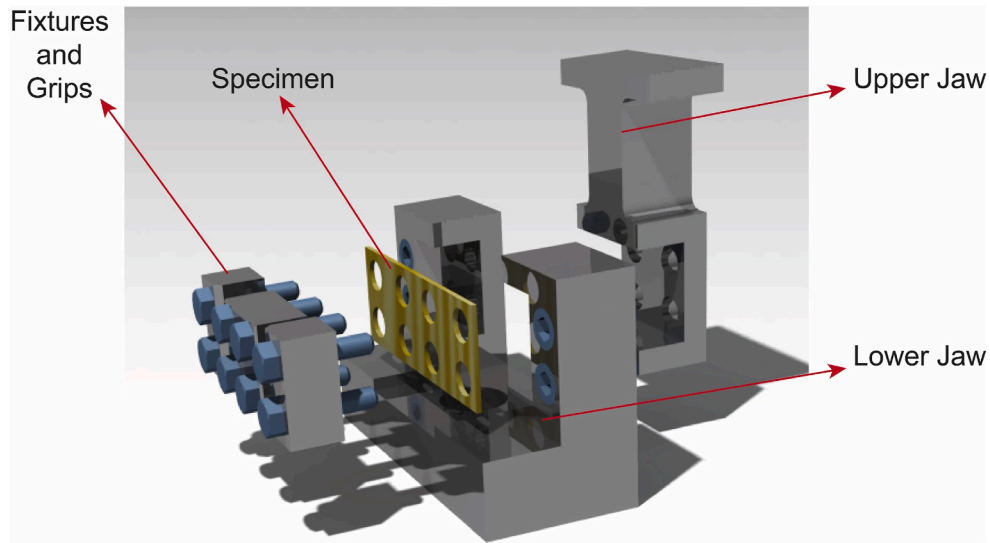
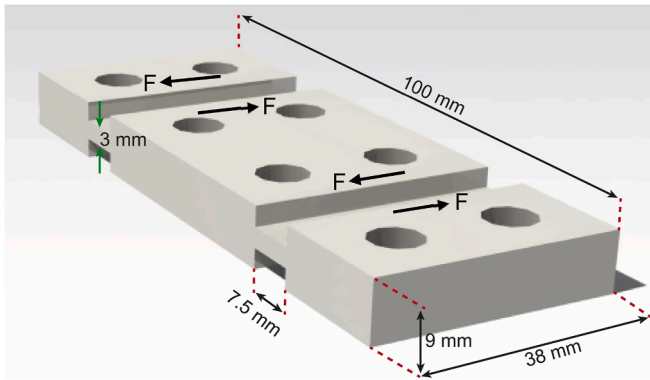**Fig. 7.** Jaw and grips components in shear test.

Fig. 8. Geometrical characteristics and dimensions of the specimen in shear test.

in-plane shear loading for understanding the presence of cut-out and its counter effects. In another research [28], failure characteristics of SMC-R composite under combined quasi-static tensile and shear tests were covered. It was summed up that, by increasing shear stress, the degree of non-linearity increased.

Modeling of the global mechanical and damage behavior of composites is necessary in design calculation of structural components [29, 30]. One can note that debonding at fiber/matrix interfaces is the main damage mechanism of SMC composites [31,32]. The Mori-Tanaka method (MTM) is a famous model for analyzing multi-phase materials and modeling the effective linear and nonlinear behavior of composites. For instance, MTM modeling could couple with finite-element calculations [33]. In SMC manufacturing process, the anisotropy is very important. The orientation distribution functions (ODFs) for SMC composites should involve information about the plane of distributed bundles (i.e. in-plane angle) [34]. One can conclude that to perform the design calculation, it is necessary to have the best experimental information under different types of loadings conditions [35].

In the present work, an experimental study is conducted for understanding the mechanical and multi-scale damage behavior of A-SMC
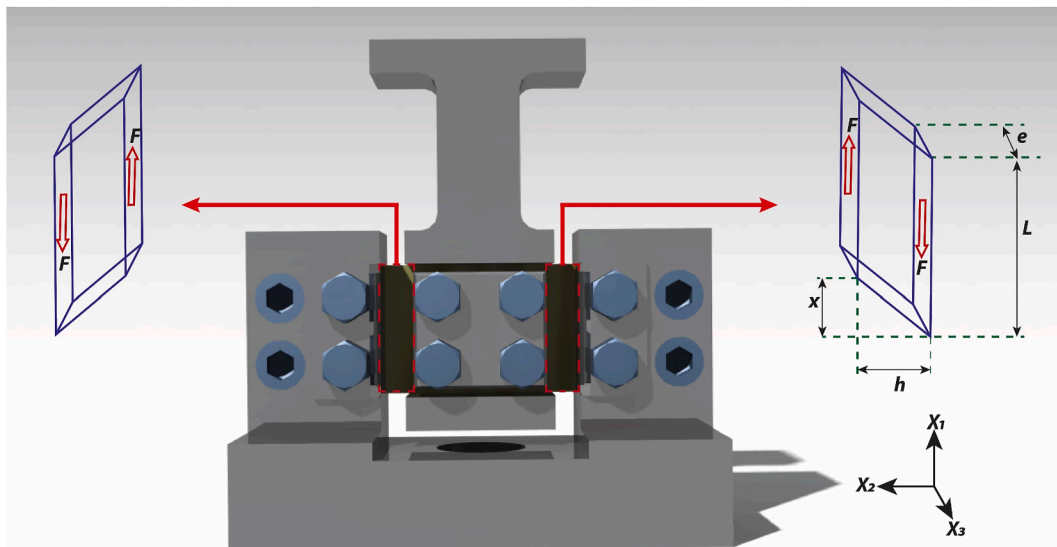

Fig. 9. Definition of reference axes and deformed parallelepipedal in the shear jaw.
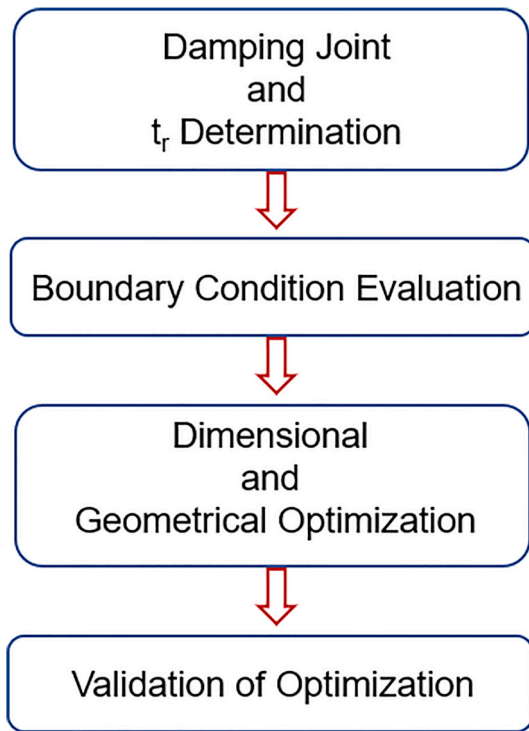
Fig. 10. Optimization steps via ABAQUS FE.

Oriented (HO) plates. In the case of Highly Oriented (HO) plate two fiber orientation configurations of HO-0° (parallel to loading direction) and HO-90° (perpendicular to loading direction) are considered. Firstly, the microstructure of A-SMC using SEM, ultrasonic test, and X-ray micro-tomography is investigated. Then, the set-ups of tension, compression and shear tests are described. An advanced tensile-base shear setup is introduced to serve pure shear test on A-SMC composite, which shear theory and the optimized specimen via ABAQUS FE code are properly explored. In the second part of this study, the effects of fiber orientation on tension, compression and shear tests are presented. In addition, different types of damage mechanisms are introduced. In part three, strain rate dependency of mechanical properties for the three types of loading are probed and an interesting comparison is made specially for the shear test to underline the influence of local damage mechanisms on the overall response of materials. Finally, to sum up the mechanisms of damage, fractography of failed A-SMC composite is observed.

composite under tension, compression, and shear loadings. The effect of loading type, fiber orientation, and strain rate have been studied. The damage mechanisms under different loading conditions and loading rates were also reported. Two types of plates have been provided by Plastic Omnium Auto Exterior: Randomly Oriented (RO) and Highly
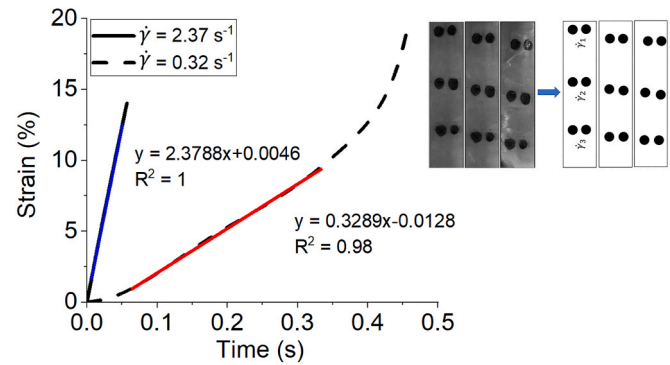

Fig. 12. Contactless strain measurement of RO-A-SMC at different strain rates in shear test.
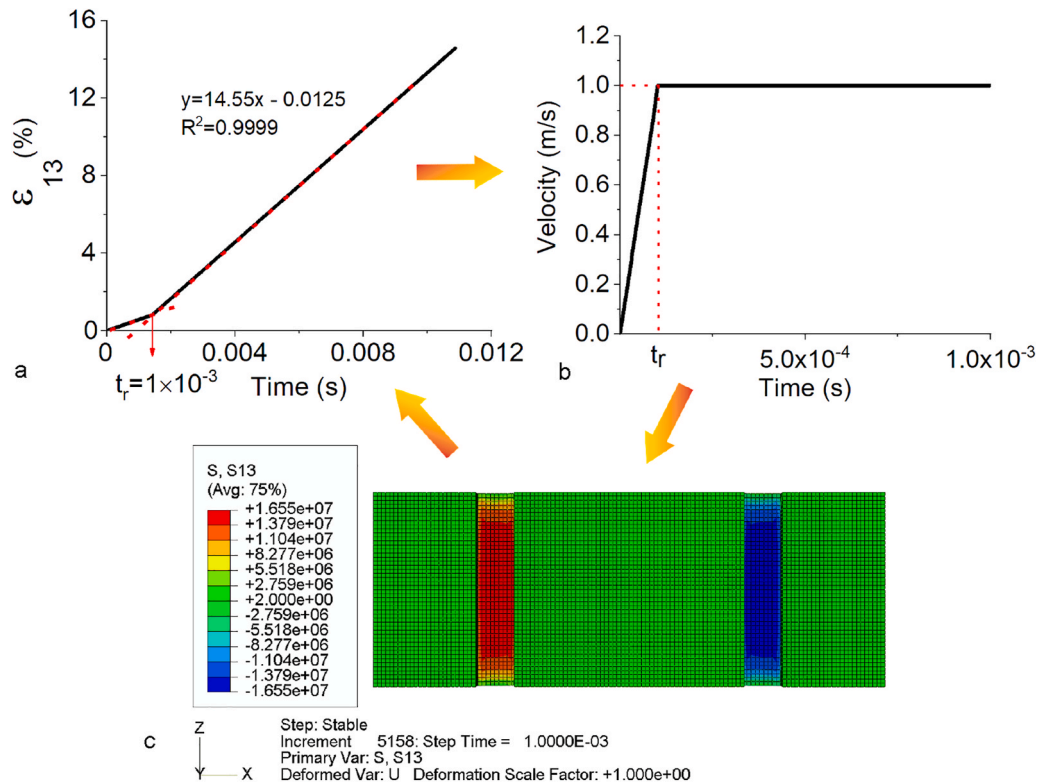

Fig. 11. Methodology of optimization in accordance with experiments and FE simulation of double rectangular gauge parts; (a) experimental data, (b) boundary conditions, (c) FE computation optimization of specimen geometry.
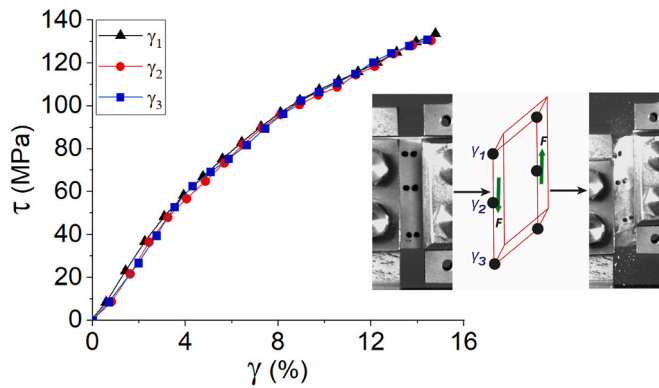
Fig. 13. Shear stress-strain curves for HO-A-SMC composite: monitoring the 6 points.

2. Materials and experimental procedure

2.1. Advanced sheet molding compound (A-SMC) composites

A-SMC is a new generation of high strength-to-weight ratio thermoset composites that is used in automotive industry, particularly for security parts. A-SMC composites are glass fiber-rich compounds, with 50% in mass corresponding to 38.5% in volume compared to the other types of SMC composites (Table 1). Moreover, they are vinyl-ester resin-based that reinforced via chopped bundles of glass fibers with a length of 25 mm. The mass production and time-efficient process of A-SMC composite is well-known and grabbed the industry's attention. In the first step, flexible and rolled raw materials cut to sheets with respect to the mold dimension and, subsequently, are stacked various layers into the molds. At the temperature of 150 °C and pressure of 60–120 kg cm^{-2} (low viscosity and cavity filling of the mold is achieved), thermo-compression process is applied. Then, materials are kept in no special reticulation for short time. Finally, consolidation phase had occurred where reticulation time included.

Two types of A-SMC plates have been prepared: Randomly Oriented (RO) and Highly Oriented (HO) plates. For HO plate, two tensile directions were chosen: HO-0° (parallel to the Mold Flow Direction (MFD))) and HO-90° (perpendicular to the MFD).

2.2. Microstructure characterization methods

2.2.1. Scanning Electron Microscopy (SEM) observation

For microstructure observation and image analysis in terms of fiber orientation and qualitative investigation of fracture mechanisms, the model of HITACHI 4800 SEM was applied.

2.2.2. X-ray micro-computed tomography (μCT)

This technique includes an X-Ray source, a rotating table, and an X-ray detector (EasyTom nano setup). The sample with a standard dimension (1 × 1 × 3 cm^3) was placed between the X-ray beam and the CCD camera detector. The μCT technique respects Beer-Lambert law ($I=I_0 e^{-\mu x}$) which showed logarithmic dependence between the initial intensity of photons "I_0" and the intensity of the transmitted photons "I" across a traveled distance "x". The attenuation coefficient "μ" describes the fraction of an X-ray beam that is absorbed or scattered per unit thickness of the sample. For a heterogeneous sample, different "μ" yields to a different intensity of the transmitted photons. Finally, the radiograph was obtained by a projection of the attenuation data along with the path of the photons. For instance, the attenuation coefficient was for selecting a radiation energy that produced the most contrast between particular materials in radiograph. For three-dimensional visualization of the materials, "μCT" combines information that provided by many radiographs, each being made from a different angle of the sample regarding the X-ray source and detector that remain fixed.

2.2.3. Ultrasonic measurement

The main purpose of establishing this technique is to better understand fiber orientation and distribution [2,37]. This measurement was taken in immersion with ultrasonic apparatus including two probes (diameter of 10 mm) of transmitting (E) and receiving (R) separated at a constant distance of "d". Moreover, the specimen was located at the angle of 45° regards to incident ultrasonic wave to create specified shear wave direction with respect to the Snell-Descart law [38]. In this method, the first stage is to measure initial velocity of ultrasonic waves in the liquid via oscilloscope for providing the flight time between two probes with the portion of distance/velocity. Then, the sample with a special thickness was perpendicularly placed between the two probes (Fig. (1-a)). Afterward, for having shear OT-wave (transversal wave), the OL-wave (longitudinal wave) should be removed that this demand
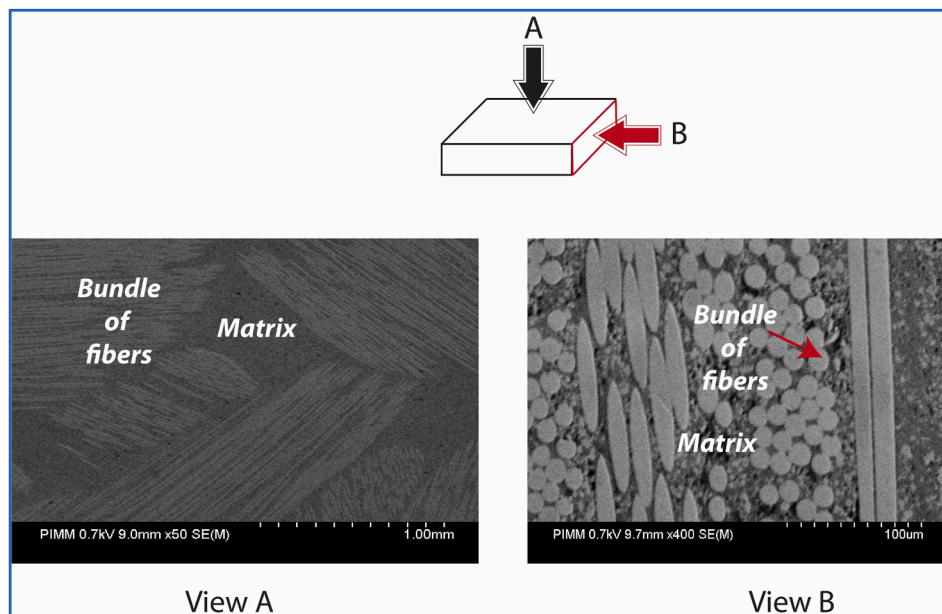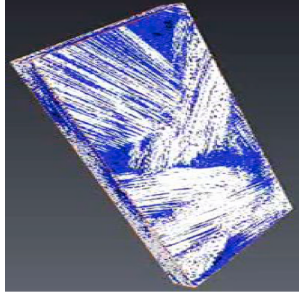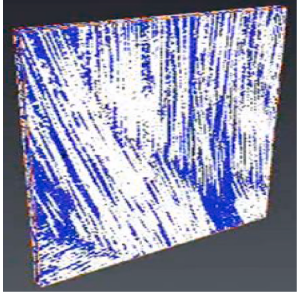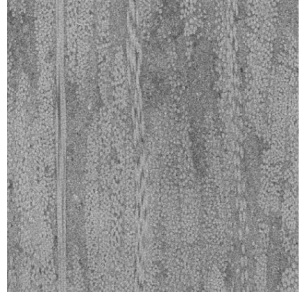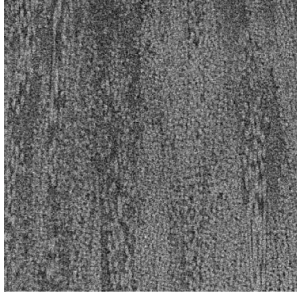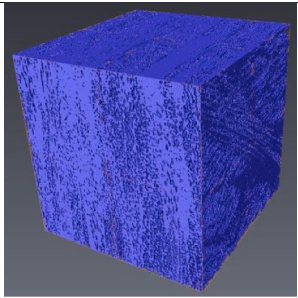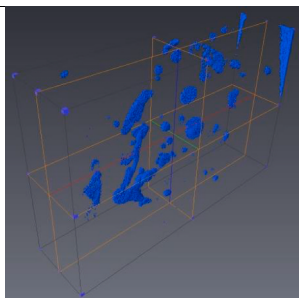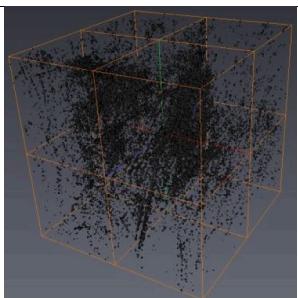

Fig. 14. Microstructure observation of RO-A-SMC composite.

Table 2
Visualization and quantitative analysis of RO-A-SMC and HO-A-SMC composites.

Section	Randomly Oriented	Volume	Highly Oriented	Volume
A-SMC		100%		100%
Fiber		47.7%		48.2%
Matrix		51.9%		50.9%
Porosity		0.3%		0.9%

was handled by sample rotation according to the incident angle "i" (Fig. (1-b)).

The procedure of ultrasonic measurement in detail has been presented in Ref. [2]. RO and HO plates with about 3 mm of thickness have been analyzed where the surface of each sample was 60×60 mm^2.

2.3. Mechanical characterizations

To understand the global mechanical behavior and related damage mechanisms of A-SMC composites, three loading configurations of tension, compression and shear in different strain rate were applied.

2.3.1. Quasi-static tensile test

The testing device was applied upon a servo-hydraulic machine manufactured via Schenk Hydropuls VHS 5020. This test could serve the crosshead speed changing from quasi-static (10^{-4} m s^{-1}) to 20 m s^{-1}. Moreover, a piezoelectric crystal load cell having a capacity of a 50 kN used to measure load level. In this investigation, different level of strain-rates was performed until failure of A-SMC composite. Fig. (2) represents an optimized device for using high strain rate tensile test that involved load cell, composite specimen, fixing system, sliding bar, hydraulic jack, damping joint (nitrile), and displacement direction [6]. Moreover, the specimen schematic illustrated in Fig. (3) that is a rectangular shape to identify damage mechanisms and progressively loss stiffness occurring during dynamic loading in mac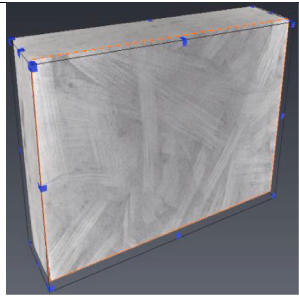ro- and micro-scale observation on gauge length (i.e. 20 mm) surface. One can note that the strain was followed by a contactless technique using high-speed camera [6].

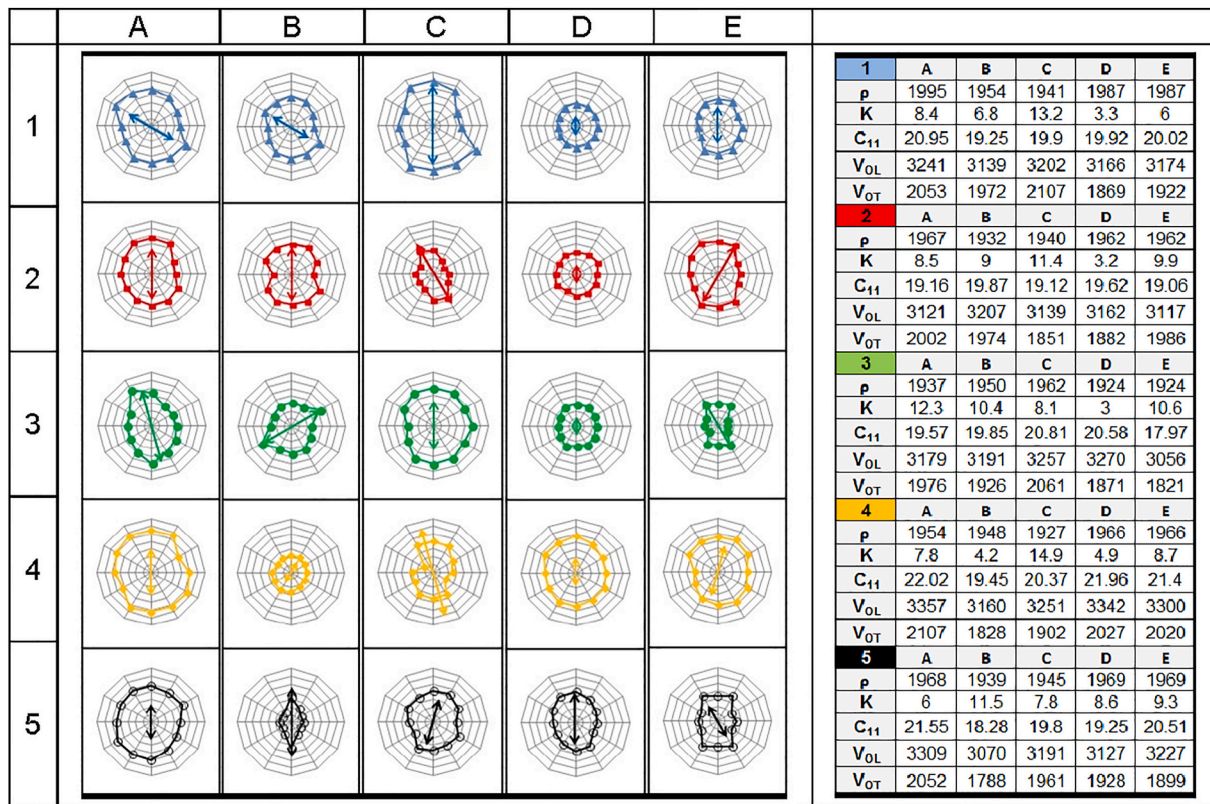|	A	B	C	D	E
1	A	B	C	D	E
ρ	1995	1954	1941	1987	1987
K	8.4	6.8	13.2	3.3	6
C_{11}	20.95	19.25	19.9	19.92	20.02
V_{OL}	3241	3139	3202	3166	3174
V_{OT}	2053	1972	2107	1869	1922
2	A	B	C	D	E
ρ	1967	1932	1940	1962	1962
K	8.5	9	11.4	3.2	9.9
C_{11}	19.16	19.87	19.12	19.62	19.06
V_{OL}	3121	3207	3139	3162	3117
V_{OT}	2002	1974	1851	1882	1986
3	A	B	C	D	E
ρ	1937	1950	1962	1924	1924
K	12.3	10.4	8.1	3	10.6
C_{11}	19.57	19.85	20.81	20.58	17.97
V_{OL}	3179	3191	3257	3270	3056
V_{OT}	1976	1926	2061	1871	1821
4	A	B	C	D	E
ρ	1954	1948	1927	1966	1966
K	7.8	4.2	14.9	4.9	8.7
C_{11}	22.02	19.45	20.37	21.96	21.4
V_{OL}	3357	3160	3251	3342	3300
V_{OT}	2107	1828	1902	2027	2020
5	A	B	C	D	E
ρ	1968	1939	1945	1969	1969
K	6	11.5	7.8	8.6	9.3
C_{11}	21.55	18.28	19.8	19.25	20.51
V_{OL}	3309	3070	3191	3127	3227
V_{OT}	2052	1788	1961	1928	1899

Fig. 15. Polar diagrams, main direction of fiber and table of characteristics in HO-A-SMC (A–E: vertical sample location and 1–5: horizontal sample location).

2.3.2. Quasi-static compression test

In this case, the testing instruments were obtained with the Instron 5881 machine (Elancourt, France) and generally contained load cell and specimen that the former part could serve 50 kN loading and velocity of 1 mm min^{-1} with respect to the NF ISO 6239 standard. In parallel, any local deformations that occurred were determined by using a camera with a capacity of 25 pictures per second. Additionally, in Fig. (4), the details of jaw and its parts illustrated. Moreover, the geometry of the specimen depicted in Fig. (5).

2.3.3. Shear test from quasi-static to high strain rates

The details of shear test set-up showed in Fig. (6) that was obtained from a servo-hydraulic test machine (Schenk Hydropuls VHS5020) in order to perform shear test by means of tensile test machine. A camera (FASTCAM-APX RS with capacity 250,000 frames per second) was placed in front of the set-up to strain measurement. For the first time in this study, a novel version of jaw (Fig. (7)) and specimen were designed to better investigate the mechanisms of failure in A-SMC composite with shear test at different strain rates. Specimen dimensions illustrated in Fig. (8) and will be explained in more details in the following sections.

2.3.3.1. Characteristics of the novel shear test method.
Based on Fig. (9), the forces and gliding planes well-demonstrated that help to define basically deformation with homogenous relative glide of parallel planes normal to the OX_2 axis along with the shear direction OX_1. The shear amount was gained via the ratio $\gamma = x/h$ which "x" is relative displacement of the parallelepiped oppose faces and "h" is the sheared width of the sample. Moreover, for providing constant shear rate, it is necessary that the opposite faces displace in a constant velocity (i.e. $\dot{X} = h\dot{\gamma}$). In this model, the shear stress is defined as $\tau = F/L.e$ and the related parameters were well-described in the schematic at ambient temperature [39]. The optimized geometry of sample was basically identified via ABAQUS FE code that will be talked more in the following sections. By the way, the main advantages of this method are simpler boundary condition, applicable for high strain rate shear test and much homogenized shear strain.

Moreover, upper jaw was fixed that allows to avoid much unwanted stress in different axes. This method, also, provides more real outcomes in shear strength evaluation due to the much volumetric engaged specimen. Indeed, more Representative Volume Elementary (RVE) were subjected to the stress, means including more defects and in-homogeneities in mechanical investigation of the composite that were made due to the unwanted production manner's error. As illustrated in Fig. (9), the fixtures and moving jaw frame were attributed to do pure injection of the stresses into the preferential sample representative volume.

2.3.3.2. Finite element (FE) optimization of specimen geometry.
ABAQUS FE optimization was used to propose the best fitted sample geometry and dimensions for shear test to reduce perturbation and disturbance wave's impact on sample, obtaining homogenous strain flowing and rapid stabilization of strain rate in the sample gauge part during the first stage of applying load by the machine. Following our previous researches [2,6], for the tensile test, the same optimization procedure was used (Fig. (10)). Finally, the geometry dimension was proposed that is much suitable for A-SMC composite.

In terms of shear test, like above-mentioned procedures, the composite assumed to be such an elastic anisotropic solid, and the results indicated the suitable dimensions in Fig. (8). Four stages of geometry optimization illustrated briefly in Fig. (10):

- **Damping joint and t_r determination:** Damping joint was placed between the sliding and hydraulic jack that could limit shock effects, which caused to a part of total imposed displacement at the beginning of the loading. This process has been activated until the end of total elastic deformation. Then, at rise time ($t_r = 1 \times 10^{-3}$ s), applied strain rate changes to a constant value and subsequently, at onward

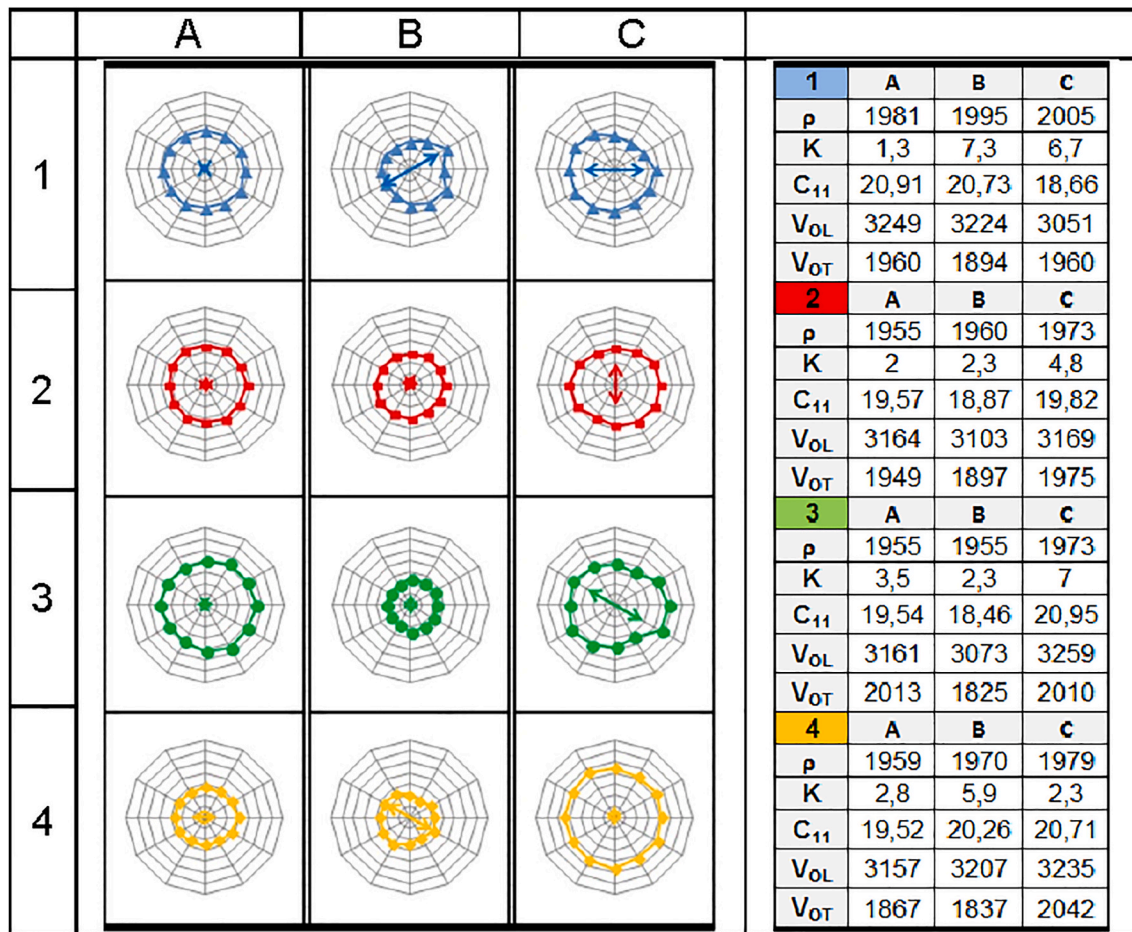| 1	A	B	C
ρ	1981	1995	2005
K	1,3	7,3	6,7
C_{11}	20,91	20,73	18,66
V_{OL}	3249	3224	3051
V_{OT}	1960	1894	1960
2	A	B	C
ρ	1955	1960	1973
K	2	2,3	4,8
C_{11}	19,57	18,87	19,82
V_{OL}	3164	3103	3169
V_{OT}	1949	1897	1975
3	A	B	C
ρ	1955	1955	1973
K	3,5	2,3	7
C_{11}	19,54	18,46	20,95
V_{OL}	3161	3073	3259
V_{OT}	2013	1825	2010
4	A	B	C
ρ	1959	1970	1979
K	2,8	5,9	2,3
C_{11}	19,52	20,26	20,71
V_{OL}	3157	3207	3235
V_{OT}	1867	1837	2042

Fig. 16. Polar diagrams, main directions of fiber and the table of the characteristics in RO-A-SMC (A–C: vertical sample location and 1–4: horizontal sample location).

t_r, the composite was induced by a constant displacement rate (Fig. (11-a)).

- **Boundary condition evaluation:** In this stage, the dynamic response of composite was examined based on imposed velocity (Fig. (11-b)). It is clear that the imposed value is raised linearly up to "t_r".
- **Dimensional and geometrical optimization:** As shown in Fig. (11-c), the aim was to optimize the specimen to serve a homogenous stress and strain field with constant strain rate within the interested zone of sample. Different width and length were analyzed that finally the dimensions presented in Fig. (8) proposed as an optimal dimension.
- **Validation of optimization:** Experimental results with numerical simulation were compared and validated the proposed dimension that will be discussed in the next section.

2.3.3.3. Associated measurement. Regarding to our last investigation [6] of high strain rate tensile test of A-SMC composite, for experimental evaluation of strain-time measurement, 6 points were marked on the face of sample for defining the initial gauge in shear test, and then changes were monitored via high-speed camera. Subsequently, image analysis was used to observe a displacement of centroid of each marked point to show the strain between the two points. Regarding the simulation and experimental results, it was proved that after damping stage, strain rate became constant that consequently could be measured from the slope of the linear part of curve in Fig. (12), which is a confirmation of the chosen boundary conditions in accordance with ABAQUS FE simulation (Fig. (11)).

Fig. (13) illustrates shear stress-strain curves for HO-A-SMC composite calculated from three points of γ_1, γ_2 and γ_3. The curves almost overlapped each other which indicates homogeneity of shear tests in addition to mentioned ABAQUS simulation in previous part (Fig. 11).

3. Results and discussion

3.1. Microstructural analysis

3.1.1. SEM observation

In this study, the A-SMC composite plates were prepared by Plastic Omnium Auto Exterior for doing tensile, compression and shear tests. Fig. (14) illustrates SEM observation of the RO-A-SMC microstructure that shows clearly randomly distribution of the fiber bundles (the length and number of fibers in each bundle are, respectively, 25 mm and 250) in matrix specially on polished cross-sectional view (view B) [3]. The microstructure of HO-A-SMC has been presented in Ref. [3].

3.1.2. X-ray micro-tomography

Table (2) illustrates µCT of RO-A-SMC microstructure in terms of skin, shell and core configuration and quantitative analysis. It is clear that in RO-A-SMC composite layers, the upper and lower specimen surfaces are slightly random in fiber orientation. In contrast, for HO-A-SMC composite, the fibers were more organized according to a special direction. Moreover, in terms of porosity, RO-A-SMC composite with 0.3% of porosity is more compact than HO-A-SMC composite, but porosity distributions are more homogenized in HO-A-SMC.

3.1.3. Ultrasonic analysis

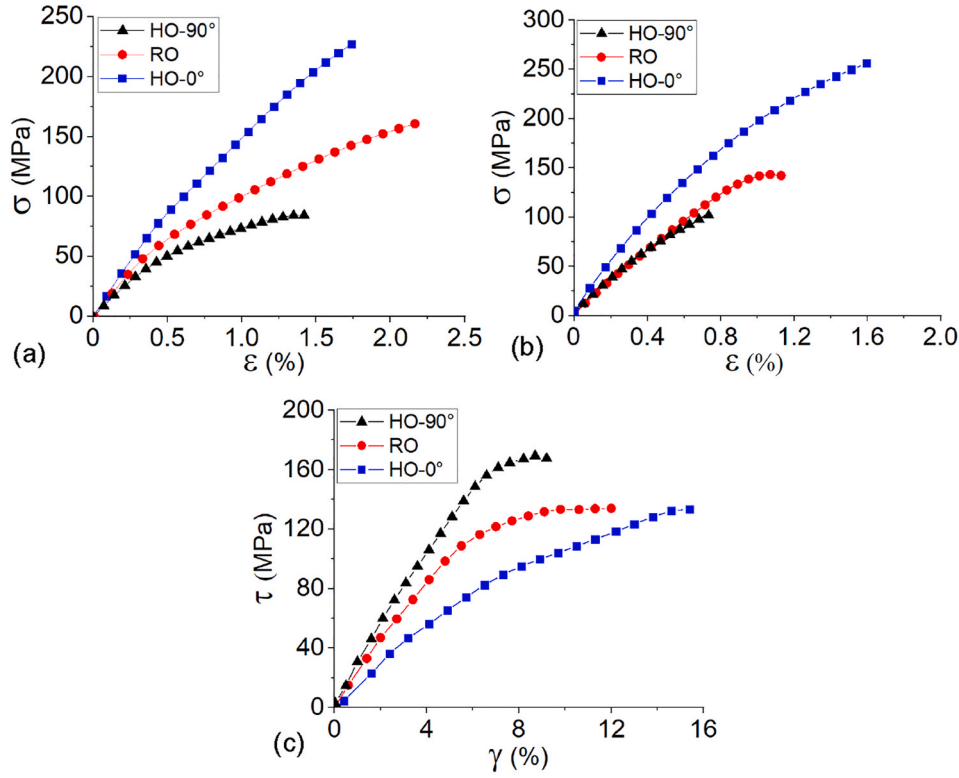Ultrasonic results were obtained in a methodology that described

Fig. 17. Stress-strain curves for (a) tension, (b) compression and (c) shear behavior of A-SMC composite with respect to the fiber orientation under quasi-static loading (i.e. 0.01 s^{-1}).
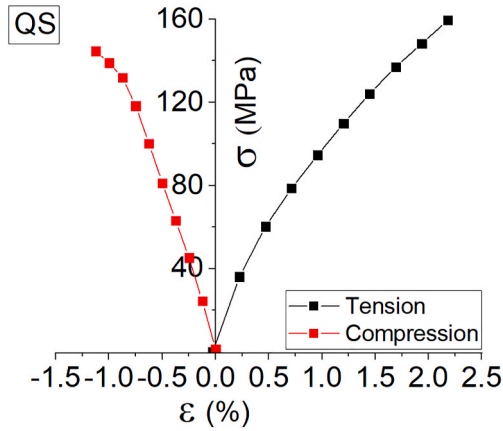

Fig. 18. Tension and compression stress-strain curves for RO-A-SMC composite.

Fig. 19. Shear stress-strain curves of RO-A-SMC at different strain rates.

above. The main factor in this technique is velocity of ultrasonic wave propagation, which is totally depends on mechanical properties and fiber orientation of sample. A parameter called acoustical birefringence (K%) was defined as:

$$K(\%) = \frac{V_{OTmax} - V_{OTmin}}{V_{OTavarage}} \times 100 \qquad (1)$$

The parameter of V_{OT} is the velocity of the shear waves for a given relative orientation θ of the composite. This coefficient represents orientation intensity, that higher amount means more oriented fibers in the matrix. The polar diagrams of velocity for RO and HO plates given in Figs. (15 and 16). As can be seen, in Fig. (15), high portion of the diagrams show special direction that there are preferred direction fibers for HO-A-SMC. However, in Fig. 16, most of the diagrams are circular that
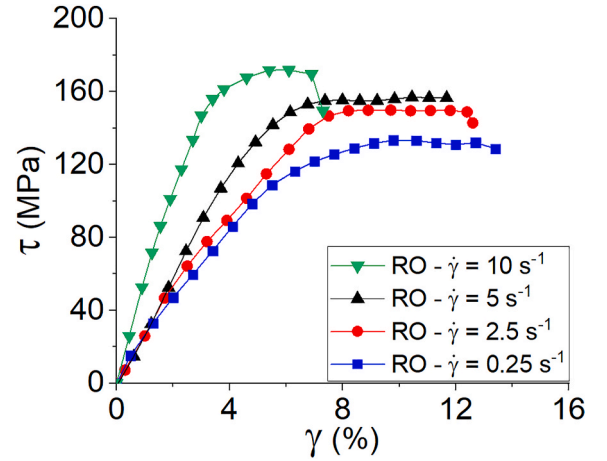
are indicating there is no preferred direction of reinforcements. Moreover, it could be understood that there is no attention-grabbing dispersion in the fiber volume fraction. Moreover, the materials seem to be an isotropic one which the characteristics of ρ (kg.m^{-3}), K (%), C$_{11}$ (GPa), V$_{OT}$ (m.s^{-1}) and V$_{OL}$ (m.s^{-1}) were measured to complete the characteristics.

3.2. Quasi-static tension, compression, and shear loadings: effect of fiber orientations

For understanding the influence of fiber orientation, HO-90°, RO, and HO-0° configurations were subjected to the tension, compression, and shear loadings in quasi-static at room temperature. According to Fig. 17, nonlinearity in stress-strain curves is obvious. In Fig. (17-a),
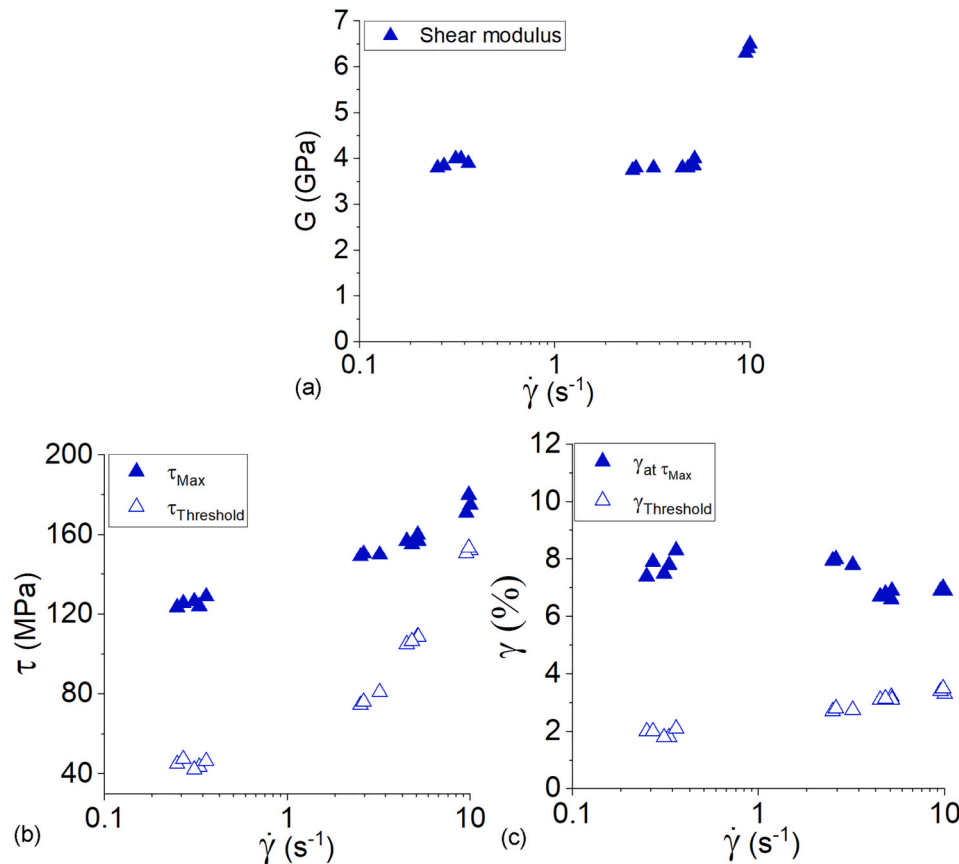
Fig. 20. Effect of strain rate on the (a) shear modulus, (b) maximum shear stress (τ_r) and threshold shear stress (τ_y), and (c) shear strain at maximum shear stress (γ_r) and threshold shear strain (γ_y) for RO-A-SMC composite.

generally, the ultimate tensile strength of HO-0° outweighed the other types and HO-90° showed lowest tensile strength. Moreover, the Young's modulus for three fiber directions of HO-90°, RO, and HO-0° were measured roughly 12.5, 14.5 and 18.5 GPa. One can note that in HO-90° most of fiber were oriented perpendicular to the loading direction. Fiber-matrix decohesion can occur when a combination of a local ultimate normal and shear stress reach on the interface of fiber/matrix. In fact, fiber-matrix interface of oriented fibers to 90° direction was failed under a pure normal stress. However, 45° oriented fibers were submitted to higher interfacial shear stress and RO configuration presented tensile strength between HO-90° and HO-0°.

In Fig. (17-b) the stress-strain behavior related to the three fiber orientations under compression loading illustrated. Similar to the tension behavior, the ultimate compression strength and strain values are higher for HO-0° than for RO and HO-90°. Moreover, the Young's modulus for three fiber directions of HO-90°, RO and HO-0° were measured roughly 16, 16 and 20 GPa. These values confirm that Youngs' modulus of A-SMC under compression loading is slightly higher than the tensile modulus. One can notice that a compression force is one that squeezes composite together. In compression loading, when fibers orientation is more in 90° to the loading direction, fiber/matrix debonding is initiated and damage is followed by matrix micro-cracking until failure. Compressive behavior of RO and HO-90° samples showed the same regime until just before failure. One can note that for RO samples, the fibers that are more parallel to the loading direction (i.e. fiber orientation ≪45°) can participate to the composite failure mechanism in addition to the decohesion of the fiber/matrix interface and matrix micro-cracking.

In Fig. (17-c), in contrast to the tension and compression, the ultimate shear strength of HO-90° is higher than HO-0°. Moreover, the Young's modulus for three fiber directions of HO-90°, RO and HO-0° are

measured roughly 3.8, 3 and 1.5 GPa. This difference is for this fact that in shear test, by applying the load in HO-0° configuration, as described before, circumferential surface of fibers was subjected to the parallelepipedal deformation and consequently shear forces caused a harsh fiber/matrix debonding. Moreover, the ultimate strain for HO-0° is higher than the others. It can be because of the role of matrix and consequently more matrix cracking until final failure. Additionally, for HO-0° configuration, the curvature reached the ultimate shear strength more smoothly than HO-90° and RO configurations. However, in the case with the fiber orientation of 90° to the loading direction, the stress was tolerated by the fibers, where the fibers resist for the high applied stress, the ultimate strength is higher for this type of orientation. In addition, fiber crack terminates the final failure and results in low strain compared to the other configurations.

The tension and compression behavior of RO-A-SMC were compared in Fig. 18 under quasi-static loading at room temperature. As can be seen, in terms of ultimate stress and failure strain, tensile values outweighed compression values by around more than 12% and 40%, respectively. Furthermore, compression modulus (about 16 GPa) is higher than tensile modulus (about 14.5 GPa). Generally, in tension test the curvature was reached the ultimate strength smoothly compared to the other one. This analysis must be completed after multi-scale damage study to understand the mechanisms under tension and compression loadings.

3.3. Effect of strain rate on shear loading

For understanding the effect of strain rate on shear behavior of RO-A-SMC, stress-strain curves in different rates from 0.25 s^{-1} to 10 s^{-1} were plotted (Fig. (19)). These curves, in general, could be divided into three sections of linear elastic behavior, damage initiation (i.e. beginning of
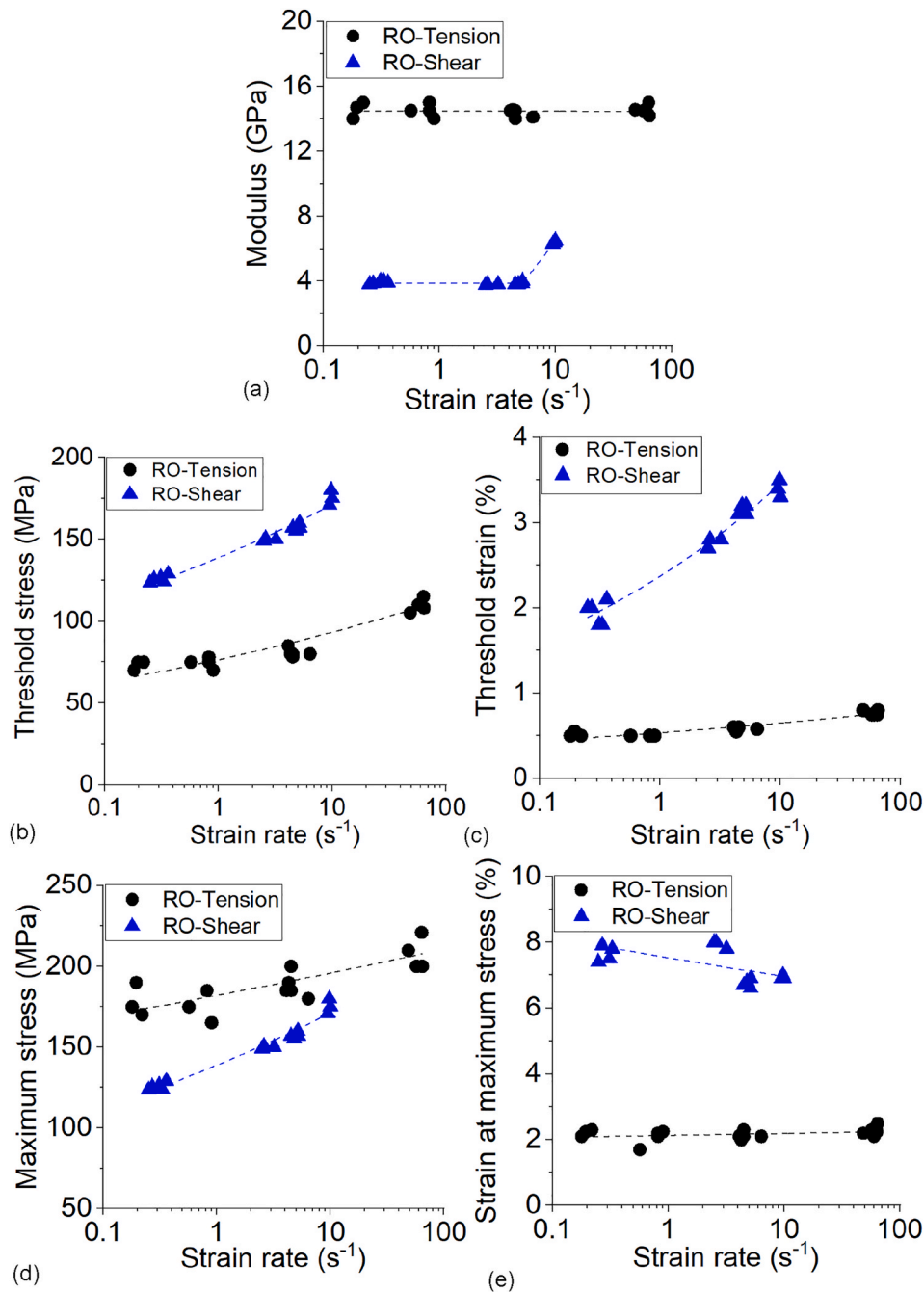
Fig. 21. Comparison of a) modulus, b) ultimate strain, c) ultimate stress, d) threshold stress, e) threshold strain after performing tensile and shear tests at different strain rates for RO-A-SMC composite.

nonlinear behavior) and damage propagation until rupture. One can observe that shear behavior of RO-A-SMC composite is strain rate dependent that by increasing the strain rate, shear modulus and ultimate shear strength are increased. For instance, under strain rate of 0.25 s^{-1}, the ultimate strain is roughly 14% which is more compared to ultimate strain under strain rate of 10 s^{-1}. Moreover, strain hardening could be observed but not as much as in high strain rate tensile test [24,40].

3.3.1. Effect of strain rate on material characteristics in shear loading

Here, materials characteristics define as shear modulus (G), shear damage thresholds related to the first non-linearity ($\tau_{\text{threshold}}$, $\gamma_{\text{threshold}}$), ultimate stress and strain (τ_{ultimate}, γ_{ultimate}) which presented in Figs. (20 and 21). The definition of ultimate characteristic is corresponding to the maximum stress level that was happened before delamination. As

illustrated in Fig. (21), shear modulus (G) is strain rate independent until shear strain rate of about 5 s^{-1}. More than this strain rates, the shear modulus drastically was increased. Moreover, other characteristics are changing with strain rate altering.

Fig. (20) indicates that by increasing the strain rate, the values of the maximum shear stress and threshold stress were increased. On the other hand, the visco-damageable behavior of RO-A-SMC is clear in shear loading. This notion has been well explained in the previous works [2,6, 41].

As demonstrated in Fig. (21) for the samples of RO-A-SMC composite, the mechanical behavior under the shear test is more strain rate dependent compared to the tensile test, especially in terms of modulus, threshold and maximum stress. The strain rate of 5 s^{-1} was known as a critical strain rate.
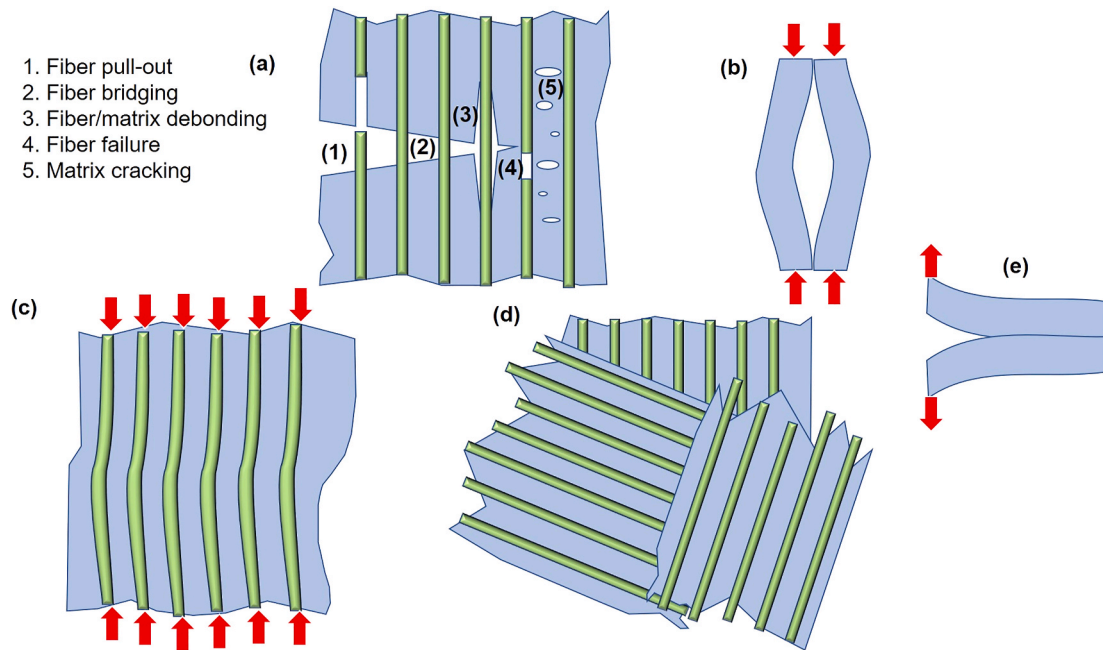
Fig. 22. Schematic of damage mechanisms in fiber-reinforced composites; (a) in-plane damage, (b) buckling delamination, (c) micro-buckling, (d) pseudo-delamination and (e) delamination [6,40].
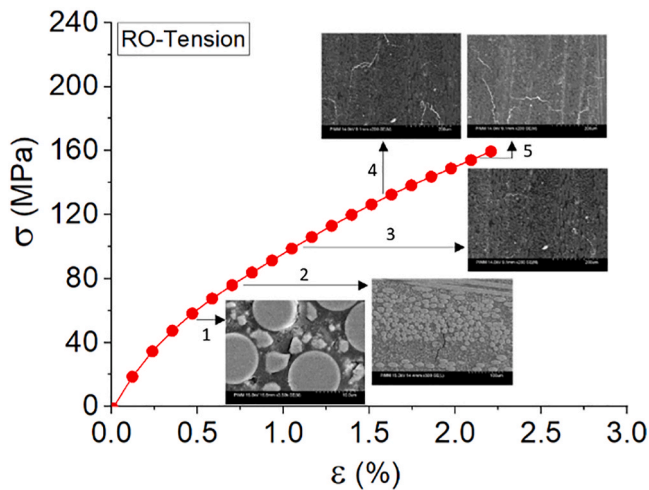

Fig. 23. Quasi-static tensile tests for RO-A-SMC composite coupled to the microstructure observation; (1): fiber/matrix debonding, (2): fiber/matrix debonding propagation and matrix micro-cracking, (3), (4) and (5): matrix micro-cracking and pseudo-delamination mechanisms [2,6,42].

Fig. (21-a) confirms modulus values under tension is higher than shear one for different strain rates (about 14.5 GPa and 4 GPa, respectively). However, the tension and shear modulus variation show the same regime until around 5 s^{-1} but after that, shear modulus value increases dramatically until 6.5 GPa for the strain rate of 10 s^{-1}. Moreover, Fig. (21-b and c) compared threshold stress values (raised from 125 GPa to 175 GPa and around 75 GPa to around 100 GPa for shear and tension loadings, respectively) and threshold strain values (increased from approximately 2%–3.5% and from 0.5% to roughly 1%, for shear and tension loadings, respectively). The slope of the threshold strain/stress increasing, for shear test are respectively 4.5 and 1.3 times more than those of tensile test. Similarly, in Fig. (21-d), the same tendency can be observed. Strain at maximum stress reveals dropping regime after the strain rate of 5 s^{-1} for shear test compared to tension test, however, for

the tension test this value is increased by strain rate increasing (Fig. (21-e)).

3.4. Multi-scale damage and fractography analysis: tensile, compression and shear loadings

A wide verity of damage mechanisms of fiber-reinforced composites were reported in Refs. [6,40] which are fiber pull-out, fiber bridging, fiber/matrix debonding, fiber failure, matrix cracking, delamination, pseudo-delamination, micro-buckling and buckling delamination (Fig. (22)). Fiber orientation, composition of composites and reinforcements, loading type, strain rate and temperature are important factors for initiation of each type of damage.

However, for understanding the types of mentioned damage mechanisms in A-SMC composites and the reasons for material characteristics respond, microstructural analysis with supplement to theoretical aspects of damage phenomenon are needed to discover. The damage threshold, type and sequence of damage stages are totally depending on sort of applied load, strain rate and fiber distribution in the matrix. As a result, multi-scale damage analysis of A-SMC composite under quasi-static tensile, compression and shear loadings were studied.

3.4.1. Tensile loading

Damage mechanisms related to the high strain rate effects on A-SMC composite were well-reported in our last researches [2,6,42]. It was concluded that depends on the fiber orientation, two main mechanisms are in competition which are fiber/matrix debonding and pseudo-delamination alongside with matrix micro-cracking based on the strain rate (Fig. (23)). As can be seen, fiber-matrix interface failure and matrix micro-cracking were obviously propagated by increasing the force under tension. In the first non-linearity stage, the fiber/matrix debonding has occurred which gradually propagated through the composite by increasing the force under tension. The later caused to the several transverse cracking of the matrix. It was proved that the decohesion at the interface of fiber/matrix is the predominant damage mechanism in RO-A-SMC under tension. Matrix breakage and pseudo-delamination can also appear for higher stress levels.

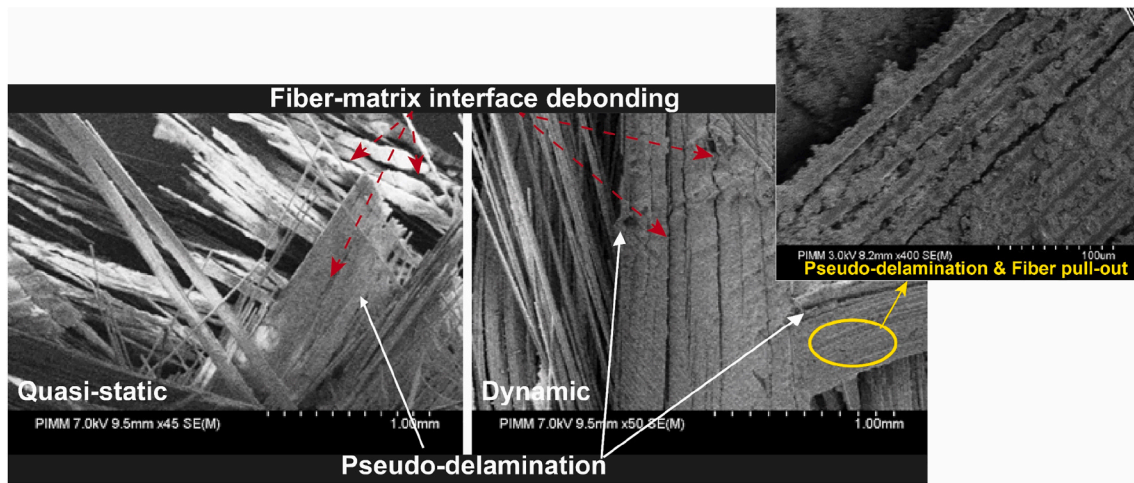Fig. (24) represents fracture surfaces of RO-A-SMC composite

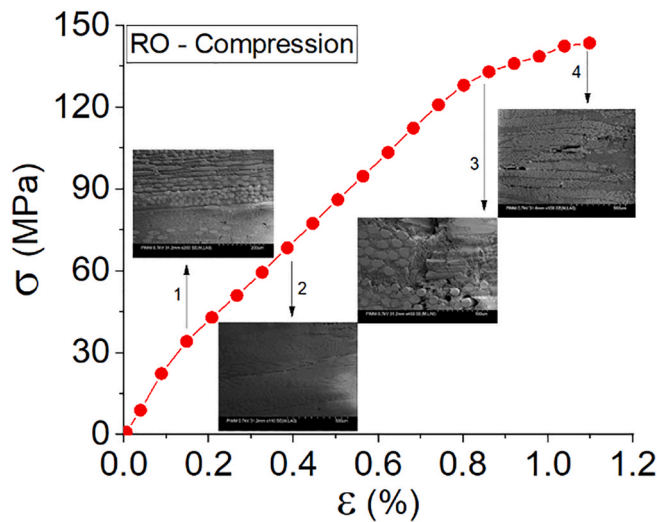Fig. 24. Fracture surfaces in RO-A-SMC composite for quasi-static and dynamic tensile loadings [2,6,42].

Fig. 25. Quasi-static compression test of RO-A-SMC coupled to the micro-structure observation;(1) decohesion at the fiber/matrix interface, (2), (3) crack propagation and (4) pseudo-delamination.

Fig. 26. Macroscopic fracture behavior of HO-A-SMC and RO-A-SMC composites under quasi-static compression loading.

subjected to the quasi-static and dynamic tensile loadings. The results of high strain rate tensile tests have been presented in previous work [6]. Both in quasi-static and dynamic fracture surface, fibers were still attached to the matrix that sum up the fact of strong fiber-matrix bonding. Moreover, in pseudo-delamination mechanisms, fibers were pulled out from each other in parallel with matrix surrounding breakage.

3.4.2. Compression loading

For damage investigation of RO-A-SMC composite, in Fig. (25), the sequence of damage evolution in compression with microstructural observation has been plotted from interrupted compression tests. In the first stage fiber/matrix interface micro-cracking was happened in fiber zone, especially in more 90° oriented to the loading direction and consequently caused crack propagation with increasing the load and subsequently pseudo-delamination observed in the final stage. It could be observed that the same scenario of damage under tension and compression loadings were come up. However, the lower values in terms of failure stress and strain under compression test are related to the test setup and limitation of deformation under compression test.

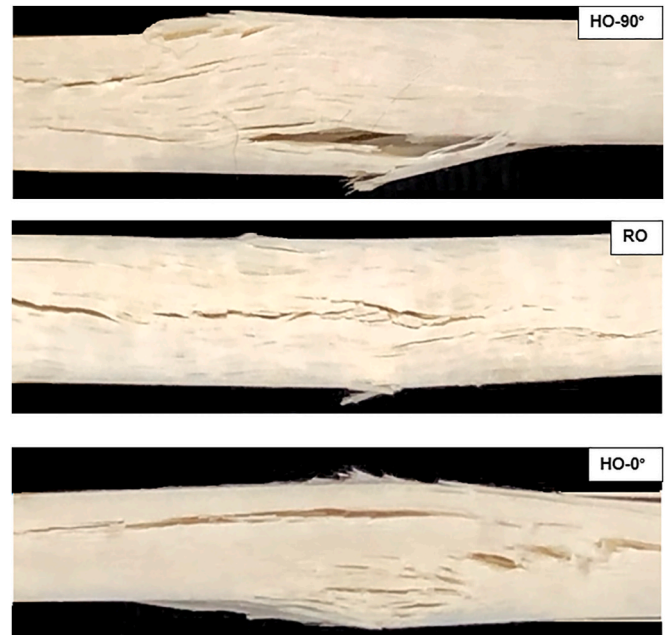Also, the macroscopic pictures presented in Fig. (26) show the

fractography under compression loading. As can be seen, pseudo-delamination was created which for HO-0° is more noticeable than the other types due to the fiber direction regarding the loading forces. However, RO-A-SMC composite behaved a moderate damage regime.

3.4.3. Shear loading

Same as other loading types, in shear test, the main damage mechanisms are fiber/matrix interface debonding and pseudo-delamination with fiber pull-out and also fiber bundle rotation which is due to the in-plane shear forces [24]. Figs. (27 and 28) illustrate these damage mechanisms of RO-A-SMC composite from interrupted shear tests. First, crack-growth happened in circumferential surface of fibers in particular for the fibers in 0° to the load direction, which is due to the parallelepipedal deformation mechanisms in shear forces that cause the formation of local stresses on fiber/matrix bonding. Then, the cracks start to grow normal to the load direction through the matrix until the final failure with pseudo-delamination mechanism.

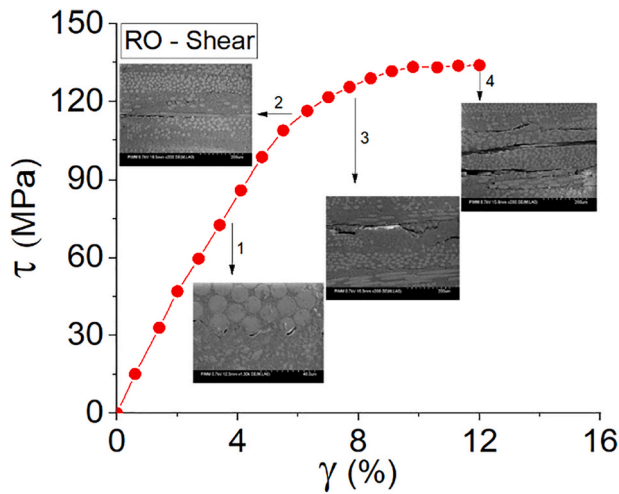However, in dynamic loading (Fig. (29)), pseudo-delamination

Fig. 27. Quasi-static shear test of RO-A-SMC composite coupled to the microstructure observation; (1) fiber/matrix debonding, (2), (3) crack propagation and (4) pseudo-delamination.

damage was more obvious which could be a reason for proving high absorption energy and good crashworthiness capability of RO-A-SMC composite. Additionally, much portion of the fibers were attached to the matrix even in high strain rate because of excellent fiber/matrix

bonding (Fig. 30). However, Fig. 29, provides a high magnification of the high strain rate fracture for showing that in final stage of fracture, matrix was a high percentage disjointed and needle-shaped fibers cause the brittle failure. It could be concluded that shear properties were clearly depended on strain rate.

4. Conclusion

Advanced sheet molding compound (A-SMC) composites are a new generation of SMC composite in terms of increased glass fibers more than 50% weight content, attracted the automobile manufacturers' interest to replace steel compounds in automobiles. The plates of Randomly Oriented (RO) and Highly Oriented (HO) with two configurations of 90° (perpendicular to MFD) and 0° (parallel to MFD) were prepared and subjected to the tension, compression, and shear loadings to understand that besides of loading types, what are the effects of fiber orientation on multi-mechanical evaluations. Moreover, different strain rates were applied to investigate the strain rate dependency of A-SMC composite according to the loading types. In terms of shear loading, a new methodology for investigation of A-SMC shear properties has been adopted. After sample optimization via ABAQUS, the samples were applied at different strain rates and compared in terms of strain rate dependency and damage mechanisms for different fiber orientations. Finally, the major conclusions are listed below:
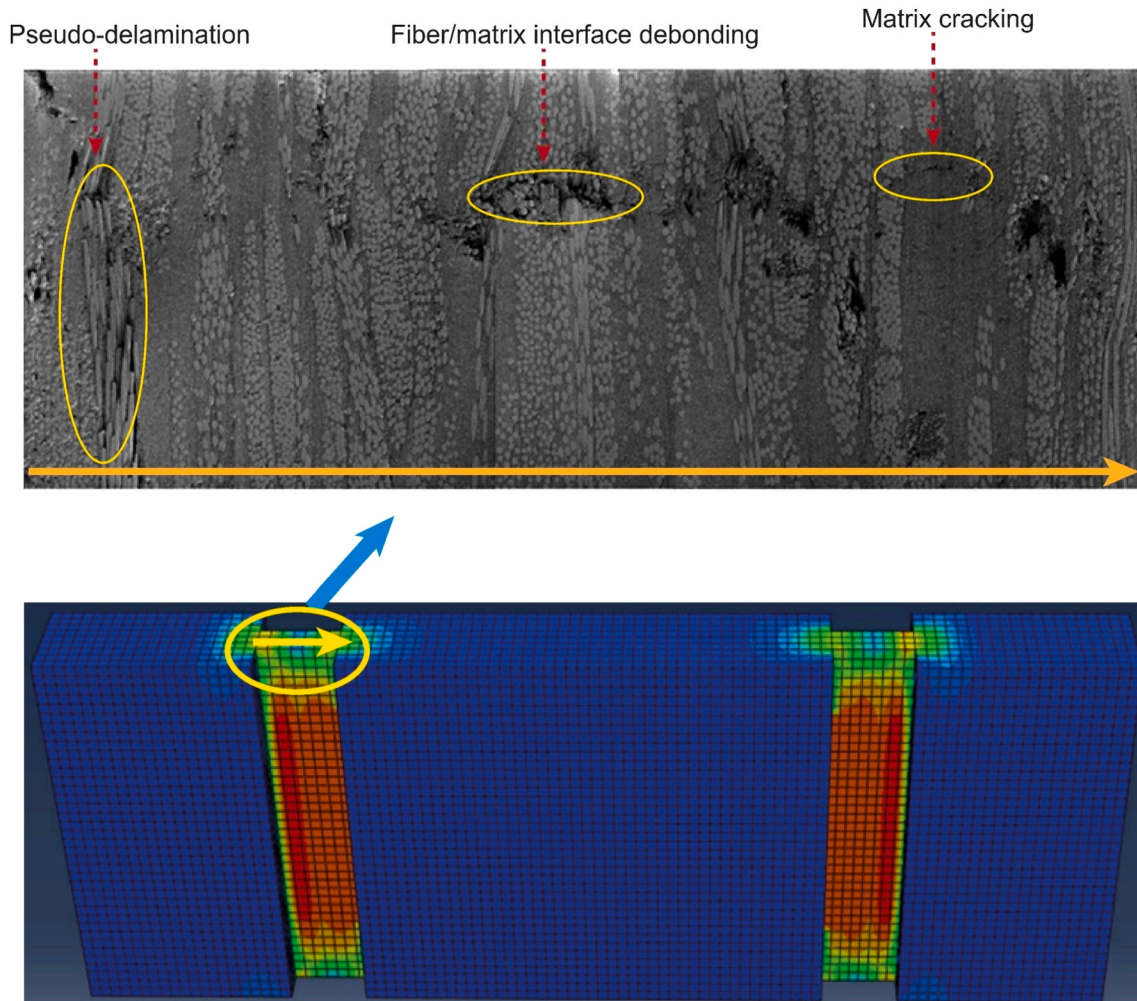

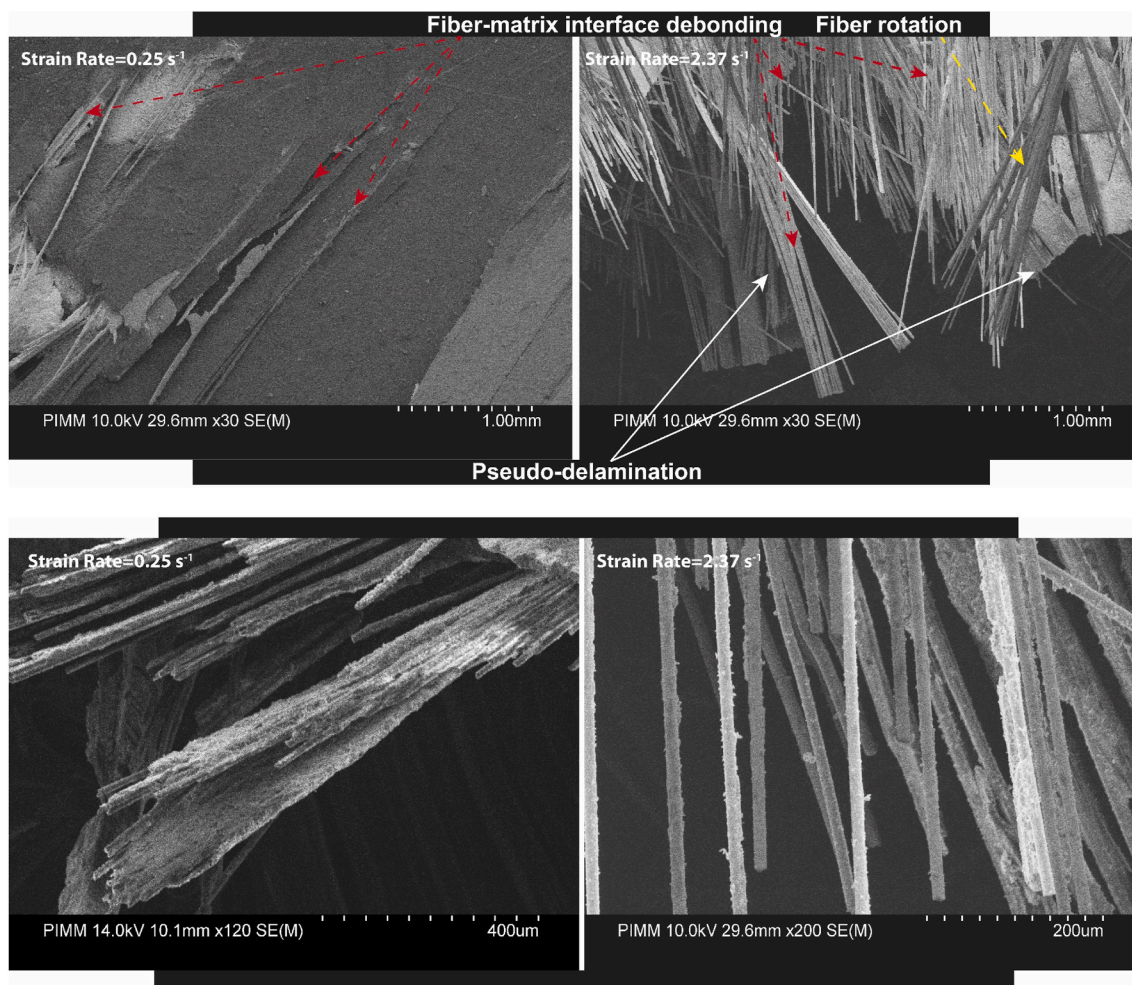**Fig. 28.** Damage phenomenon in of A-SMC composite under shear loading.

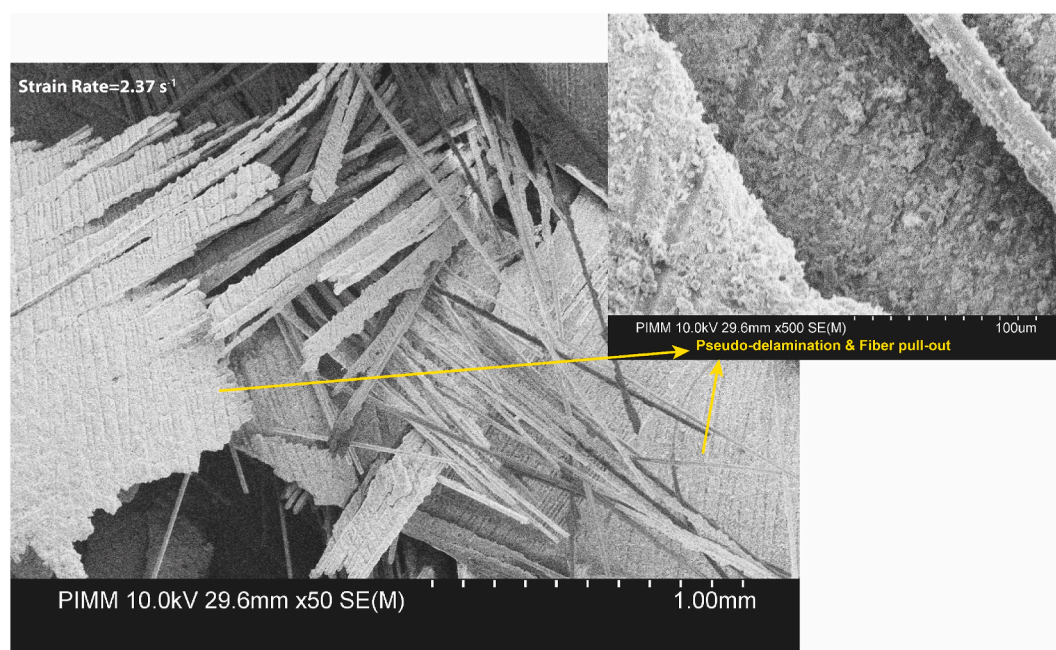**Fig. 29.** Fractography of RO-A-SMC composite under quasi-static and dynamic shear loading.

Fig. 30. Pseudo-delamination of high strain shear test in RO-A-SMC.

- Shear setup and specimen dimension were properly designed and optimized by comparing ABAQUS FE codes and experimental results with a damping time of 1×10^{-3} s.
- Different damage mechanisms of A-SMC composites are fiber pull-out, fiber failure, pseudo-delamination, fiber/matrix debonding, buckling, etc. Among them, based on the strain rate and loading types, fiber/matrix debonding, matrix cracking and pseudo-delamination were competing.
- The effect of fiber orientation on global mechanical behavior showed that in tension and compression tests, HO-0° A-SMC composite represented higher strength but HO-90° configuration presented higher shear strength compared to the HO-0° and RO composite due to the parallelepipedal deformation.
- For strain rate effects on tension, compression and shear tests, the dependency of mechanical properties (i.e. ultimate strength and ultimate strain) was well-proved. Although Young modulus was not strain rate sensitive. Shear modulus (G) was strain rate-independent until shear strain rate of about 5 s^{-1}. More than this strain rate value, the shear modulus drastically was increased.
- In fractography by SEM observation, it was presented that by increasing strain rate (for instance in shear test: from 0.25 s^{-1} to 2.37s^{-1}), matrix in high percentage was disjointed and fiber brittle failure was happened.

Declarations

- **Consent to participate:** Not applicable.
- **Consent to publish:** Not applicable.
- **Conflict of interest**: The authors declare that they have no conflicts of interest.

Declaration of competing interest

The authors declare that they have no known competing financial interests or personal relationships that could have appeared to influence the work reported in this paper.

References

[1] https://ec.europa.eu/clima/policies/transport/vehicles/regulation_en n.d.

[2] Shirinbayan M, Fitoussi J, Abbasnezhad N, Meraghni F, Surowiec B, Tcharkhtchi A. Mechanical characterization of a low density sheet molding compound (LD-SMC): multi-scale damage analysis and strain rate effect. Compos B Eng 2017;131:8–20. https://doi.org/10.1016/j.compositesb.2017.08.004.

[3] Shirinbayan M, Fitoussi J, Bocquet M, Meraghni F, Surowiec B, Tcharkhtchi A. Multi-scale experimental investigation of the viscous nature of damage in Advanced Sheet Molding Compound (A-SMC) submitted to high strain rates. Compos B Eng 2016;115.

[4] Yalcin B. 5 - hollow glass microspheres in sheet molding compounds. In: Amos SE, Yalcin B, editors. Hollow glas. Microspheres plast. Elastomers, adhes. Compd. Oxford: William Andrew Publishing; 2015. p. 123–45. https://doi.org/10.1016/B978-1-4557-7443-2.00005-0.

[5] Shirinbayan M, Fitoussi J, Meraghni F, Surowiec B, Laribi M, Tcharkhtchi A. Coupled effect of loading frequency and amplitude on the fatigue behavior of advanced sheet molding compound (A-SMC). J Reinforc Plast Compos 2016.

[6] Shirinbayan M, Fitoussi J, Meraghni F, Surowiec B, Bocquet M, Tcharkhtchi A. High strain rate visco-damageable behavior of Advanced Sheet Molding Compound (A-SMC) under tension. Compos B Eng 2015;82:30–41. https://doi.org/10.1016/j.compositesb.2015.07.010.

[7] Jacob GC, Fellers JF, Simunovic S, Starbuck JM. Energy absorption in polymer composites for automotive crashworthiness. J Compos Mater 2002;36:813–50.

[8] Abbasnezhad N, Khavandi A, Fitoussi J, Arabi H, Shirinbayan M, Tcharkhtchi A. Influence of loading conditions on the overall mechanical behavior of polyether-ether-ketone (PEEK). Int J Fatig 2018;109:83–92. https://doi.org/10.1016/j.ijfatigue.2017.12.010.

[9] Baste S, Gérard A. Evaluation of anisotropic damage in composite materials. Eval Anisotropic Damage Compos Mater 1994;3.

[10] Jendli Z, Fitoussi J, Meraghni F, Baptiste D. Anisotropic strain rate effects on the fibre-matrix interface decohesion in sheet moulding compound composites. Compos Sci Technol 2005;65:387–93.

[11] Asadi A, Baaij F, Mainka H, Rademacher M, Thompson J, Kalaitzidou K. Basalt fibers as a sustainable and cost-effective alternative to glass fibers in sheet molding compound (SMC). Compos B Eng 2017;123:210–8. https://doi.org/10.1016/j.compositesb.2017.05.017.

[12] Dumont P, Orgéas L, Favier D, Pizette P, Venet C. Compression moulding of SMC: in situ experiments, modelling and simulation. Composer Part A Appl Sci Manuf 2007;38:353–68.

[13] Kim MS, Lee W Il, Han WS, Vautrin A. Optimisation of location and dimension of SMC precharge in compression moulding process. Comput Struct 2011;89:1523–34. https://doi.org/10.1016/j.compstruc.2011.04.004.

[14] Kim DK, Choi HY, Kim N. Experimental investigation and numerical simulation of SMC in compression molding. J Mater Process Technol 1995;49:333–44.

[15] Park CH, Lee WI, Yoo YE, Kim EG. A study on fiber orientation in the compression molding of fiber reinforced polymer composite material [J]. J Mater Process Technol 2001;111:233–9.

[16] Mostafa A, Shankar K, Morozov EV. Insight into the shear behaviour of composite sandwich panels with foam core. Mater Des 2013;50:92–101. https://doi.org/10.1016/j.matdes.2013.03.016.

[17] Dargahi A, Sedaghati R, Rakheja S. On the properties of magnetorheological elastomers in shear mode: design, fabrication and characterization. Compos B Eng 2019;159:269–83. https://doi.org/10.1016/j.compositesb.2018.09.080.

[18] Kellar EJC, Abbey KJ, Burchardt B, White CC, Tan K, Wolf AT, et al. Contributor contact details. In: Dillard DA, editor. Adv. Struct. Adhes. Bond. Woodhead Publishing; 2010. https://doi.org/10.1016/B978-1-84569-435-7.50022-5. xiii–xvi.

[19] Astm D. 3165-07: standard test method for strength properties of adhesives in shear by tension loading of single-lap-joint laminated assemblies. Annu Book ASTM Stand 2014;15(6):213–6 [n.d].

[20] DIN EN 2563:1997-03, Luft- und Raumfahrt.- Kohlenstoffaserverstärkte Kunststoffe.- Unidirektionale Laminate; Bestimmung der scheinbaren interlaminaren Scherfestigkeit. Deutsche fassung EN_2563:1997. Beuth Verlag GmbH; 1997. https://doi.org/10.31030/7253947 n.d.

[21] ASTM D2344/D2344M-00 standard test method for short-beam strength of polymer matrix composite materials and their laminates. West Conshohocken, PA: ASTM International; 2016 [n.d].

[22] Botelho EC, Figiel Ł, Rezende MC, Lauke B. Mechanical behavior of carbon fiber reinforced polyamide composites. Compos Sci Technol 2003;63:1843–55. https://doi.org/10.1016/S0266-3538(03)00119-2.

[23] G'Sell C, Boni S, Shrivastava S. Application of the plane simple shear test for determination of the plastic behaviour of solid polymers at large strains. J Mater Sci 1983;18:903–18. https://doi.org/10.1007/BF00745590.

[24] Shokrieh MM, Omidi MJ. Investigation of strain rate effects on in-plane shear properties of glass/epoxy composites. Compos Struct 2009;91:95–102. https://doi.org/10.1016/j.compstruct.2009.04.035.

[25] Holmes J, Das R, Stachurski Z, Compston P, Kalyanasundaram S. Development of an S-specimen geometry for shear testing of woven thermoplastic composites. Compos B Eng 2020;203:108485. https://doi.org/10.1016/j.compositesb.2020.108485.

[26] Jia Z, Yuan Q, Feng X, Zou Y, Yu J. Shear properties of polyurethane ductile adhesive at low temperatures under high strain rate conditions. Compos B Eng 2019;156:292–302. https://doi.org/10.1016/j.compositesb.2018.08.060.

[27] Kolanu NR, Raju G, M R. Damage assessment studies in CFRP composite laminate with cut-out subjected to in-plane shear loading. Compos B Eng 2019;166:257–71. https://doi.org/10.1016/j.compositesb.2018.11.142.

[28] Urapakam Ramakrishnan M, Mallick PK. Strength and failure characteristics of a glass fiber SMC-R composite under combined tensile and shear stresses. Compos B Eng 2019;176:107141. https://doi.org/10.1016/j.compositesb.2019.107141.

[29] Chatzigeorgiou G, Seidel GD, Lagoudas DC. Effective mechanical properties of "fuzzy fiber" composites. Compos B Eng 2012;43:2577–93. https://doi.org/10.1016/j.compositesb.2012.03.001.

[30] Tan W, Liu B. A physically-based constitutive model for the shear-dominated response and strain rate effect of carbon fibre reinforced composites. Compos B Eng 2020;193:108032. https://doi.org/10.1016/j.compositesb.2020.108032.

[31] Cherkaoui M, Sabar H, Berveiller M. Elastic composites with coated reinforcements: a micromechanical approach for nonhomothetic topology. Int J Eng Sci 1995;33:829–43. https://doi.org/10.1016/0020-7225(94)00108-V.

[32] Christensen RM. Mechanics of composite materials. Dover Publications; 2012.

[33] Stupkiewicz S, editor. Fundamentals of micromechanics BT - micromechanics of contact and interphase layers. Berlin, Heidelberg: Springer Berlin Heidelberg; 2007. p. 7–16. https://doi.org/10.1007/978-3-540-49717-2_2.

[34] Anagnostou D, Chatzigeorgiou G, Chemisky Y, Meraghni F. Hierarchical micromechanical modeling of the viscoelastic behavior coupled to damage in SMC and SMC-hybrid composites. Compos B Eng 2018;151:8–24. https://doi.org/10.1016/j.compositesb.2018.05.053.

[35] Fitoussi J, Meraghni F, Jendli Z, Hug G, Baptiste D. Experimental methodology for high strain-rates tensile behaviour analysis of polymer matrix composites. Compos Sci Technol 2005;65:2174–88.

[36] Laribi MA, TieBi R, Tamboura S, Shirinbayan M, Tcharkhtchi A, Dali H Ben, et al. Sheet molding compound automotive component reliability using a micromechanical damage approach. Appl Compos Mater 2020;27:693–715. https://doi.org/10.1007/s10443-020-09831-5.

[37] Schladitz K, Büter A, Godehardt M, Wirjadi O, Fleckenstein J, Gerster T, et al. Non-destructive characterization of fiber orientation in reinforced SMC as input for simulation based design. Compos Struct 2017;160:195–203. https://doi.org/10.1016/j.compstruct.2016.10.019.

[38] Dupertuis MA, Proctor M, Acklin B. Generalization of complex snell–descartes and fresnel laws. J Opt Soc Am A 1994;11:1159–66. https://doi.org/10.1364/JOSAA.11.001159.

[39] Paupler PGE. Dieter. Mechanical metallurgy. third ed., 23. New York: Mc Graw-Hill Book Co.; 1986. p. 194. https://doi.org/10.1002/crat.2170230211. XXIII + 751 pp., DM 138.50, ISBN 0–07–016893–8. Cryst Res Technol 1988.

[40] Anderson TL. Fracture mechanics: fundamentals and applications. fourth ed., 76; 2017.

[41] Shirinbayan M, Fitoussi J, Abbasnezhad N, Lucas A, Tcharkhtchi A. Multi-scale damage and mechanical behavior of sheet molding compound composites subjected to fatigue , dynamic , and post-fatigue dynamic. 2019.

[42] Shirinbayan M, Fitoussi J, Bocquet M, Meraghni F, Surowiec B, Tcharkhtchi A. Multi-scale experimental investigation of the viscous nature of damage in Advanced Sheet Molding Compound (A-SMC) submitted to high strain rates. Compos B Eng 2017;115:3–13. https://doi.org/10.1016/j.compositesb.2016.10.061.